

Nanostructured Titanium with Ultrafine-Grained Structure as Advanced Engineering Material for Biomedical Application

Luiza R. Rezyapova, Zarema A. Safargalina, Emil I. Usmanov, Roman R. Valiev, Timur B. Minasov, and Ruslan Z. Valiev*

This article is dedicated to the anniversary of Prof. Reinhard Pippan, who has made significant contributions to the research and development of severe plastic deformation techniques, particularly high pressure torsion, for the production of nanostructured materials

Titanium and its alloys are popular materials for medical application, particularly in implant devices, where high mechanical properties and osseointegration are critical factors for successful implantation. In this work, the progress in the studies of nanostructured commercially pure Grade 4 titanium (nanoTi) is demonstrated, in which an ultrafine-grained structure with nanoscale grain size is formed using severe plastic deformation processing. Nanostructured Grade 4 Ti has a very high strength, and its physical nature and strengthening mechanisms are analyzed herein. NanoTi proved also to have very high osseointegration during in vivo experiments. At the same time, the highest biofunctionality is demonstrated by the etched nanoTi samples with pronounced surface roughness, the latter being revealed from precise roughness measurements. The present study provided convincing evidence of accelerated bone formation on nanoTi, which is very promising for manufacture of dental and maxillofacial implants.

demonstrate that nanostructured commercially pure titanium (nanoTi) attracts and retains interest as a very promising material for biomedical applications.^[1–3] The formation of ultrafine-grained (UFG) structure with the grain size in the nano- and/or submicron range using severe plastic deformation (SPD) techniques allows for very high strength and fatigue life in titanium, the values of which are noticeably higher even than in titanium alloys.^[1,3,4] As shown in a recent study,^[5] it was possible to produce CP Ti Grade 4 with ultimate tensile strength (UTS) $\sigma_u > 1500$ MPa using processing by high pressure torsion (HPT). In this article, we examine the physical nature of such superstrength and apply the developed approach to man-

ufacture high-strength titanium rods, which are further used for implantable devices of improved design. Moreover, the absence of significant amount of alloying elements in commercially pure titanium makes this material the most attractive for providing its increased osseointegration. Various factors may affect osseointegration of implants including the material used in the implant, its biocompatibility, processing conditions, surface topography of the implant, surgical technique, and other. These research trends are supported by the results of some in vitro and in vivo tests that are available for nanoTi today.^[2,6] At the same time, osseointegration properties are closely related to the surface modification of the material, formation of a specific topography and/or application of a bioactive coating.^[7,8] As is known, sandblasting and subsequent acid etching are commonly used for implants made of titanium materials.^[7–10] However, there is not yet common understanding how surface modification influences biofunctionality of the nanostructured materials. The aim of this work is to compare osseointegration properties of titanium implant samples having different grain sizes (crystallites) and different surface treatments.

1. Introduction

In the recent years, research and development of titanium and its alloys in medical and health care goods convincingly

L. R. Rezyapova, Z. A. Safargalina, E. I. Usmanov, R. R. Valiev, R. Z. Valiev
Institute of Physics of Advanced Materials
Ufa University of Science and Technology
32 Zaki Validi St., Ufa 450076, Russia
E-mail: ruslan.valiev@ugatu.su

Z. A. Safargalina, R. R. Valiev, R. Z. Valiev
Laboratory for Dynamics and Extreme Characteristics of Promising
Nanostructured Materials
Saint Petersburg State University
28 University Ave., St. Petersburg 198504, Russia

T. B. Minasov
Department of Traumatology and Orthopaedics
Bashkir State Medical University
2a Teatralnaya St., Ufa 450000, Russia

 The ORCID identification number(s) for the author(s) of this article can be found under <https://doi.org/10.1002/adem.202400394>.

DOI: 10.1002/adem.202400394

2. Results

2.1. Microstructure and Mechanical Properties

As noted previously, currently, HPT is deemed one of the most efficient techniques for microstructure refinement of titanium, allowing for the formation of a structure with grain sizes of about 100 nm and a larger fraction of high-angle boundaries.^[11] Additionally, HPT typically results in the formation of segregations of alloying elements at grain boundaries, as well as the appearance of nanoclusters and/or highly dispersed second-phase precipitates.^[12–15] These nanostructural features and UFG structure additionally contribute to the strength of materials. Herein, with the use of this approach we analyze experimental studies^[5] that contribute to establishing the nature of the superstrength state of HPT-processed CP Grade 4 titanium.

The microstructure of CP Grade 4 titanium in initial hot-rolled state had a grain shape with an average size of $8.3 \pm 0.9 \mu\text{m}$. Some extended (2–3 μm) localized β -phase particles with a width of about 1 μm and intermetallic particles Ti_2Fe , rounded in shape with sizes less than 0.6 μm , were observed along the grain boundaries. The material exhibited typical Grade 4 titanium strength and ductility parameters - with yield strength (YS) and UTS of 500 ± 40 and 680 ± 10 MPa, respectively. The relative elongation did not exceed $23.9 \pm 1.4\%$.

As is noted in Section 5, for the formation of a nanostructured state in Grade 4 titanium with varying defect densities, such as

nano-sized precipitates and dislocation densities, the samples were subjected to combined deformation by HPT and heat treatment at 700 and 350 °C.^[5] The experimental data are provided in **Figure 1**.

TEM and XRD analysis of the structure revealed that the combined treatment resulted in the formation of various nanodisperse phases, depending on the treatment modes (Figure 1a). Particularly, HPT + annealing at 700 °C + HPT + annealing at 350 °C lead to the formation of a nanostructured state in Grade 4 titanium. The average grain size was 100 ± 10 nm, and there were nanosized particles of β -phase and intermetallic Ti_2Fe with average sizes of 90 ± 10 and 22 ± 2 nm respectively (Figure 1b,c). The volume fractions of β -phase and Ti_2Fe were $3.0 \pm 1.0\%$ and $1.1 \pm 0.1\%$, respectively. Therefore, by using HPT with different types of annealing, a state with UFG structure and nanodispersed particles may be formed in Grade 4 titanium.

The structural parameters of Ti measured by X-ray and TEM analysis after processing are summarized in **Table 1**.

Figure 1d shows the stress–strain engineering curves of the samples during tensile tests. In the initial state, the character of the curve is typical for the materials obtained by hot rolling. After reaching the yield point, a gradual increase in stresses to maximum values is observed, followed by a decrease due to strain localization. The character of the curve changes significantly after HPT. A decrease in the uniform strain, a significant increase in the strength parameters and a decrease in ductility

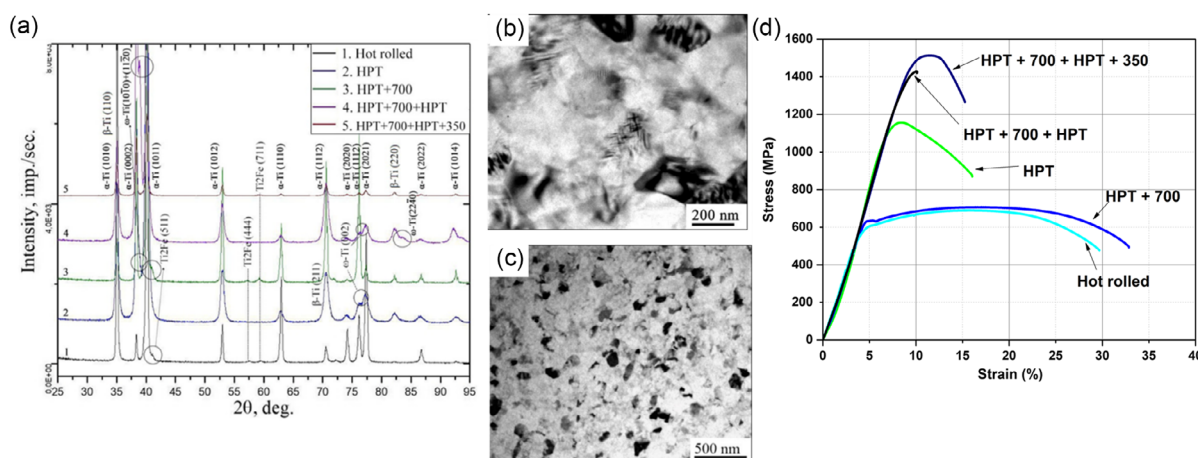


Figure 1. a) Structural studies and mechanical properties of Grade 4 titanium after different stages of thermomechanical treatment: diffractograms; b,c) bright-field TEM images after HPT + 700 °C + HPT + 350 °C; d) engineering stress–strain curves. Adapted with permission.^[5] Copyright 2023, Pleiades Publishing, Ltd.

Table 1. Structural parameters of CP Ti Grade 4 after various processing regimes.

State	Average grain size, d [μm]	Total dislocation density, ρ [m^{-2}]	Size of second-phase particles, r [nm]	Volume fraction of second-phase particles, f [%]
Hot rolled	10.00 ± 2.00	$\approx 2.4 \times 10^{14}$	10^3	2–3
HPT	0.12 ± 0.03	$\approx 2.1 \times 10^{15}$	–	<1
HPT + 700	5.00 ± 1.00	$\approx 2.2 \times 10^{14}$	35 ± 7	4–5
HPT + 700 + HPT	0.09 ± 0.03	$\approx 1.6 \times 10^{15}$	–	<1
HPT + 700 + HPT + 350	0.12 ± 0.04	$\approx 2.3 \times 10^{14}$	18 ± 10	7–8

are observed. High-temperature annealing of the deformed state leads to the development of recrystallization and complete leveling of the hardening effect from the formation of the UFG structure and distortions of the crystal lattice. Additional HPT leads to a rapid increase in the material strength but a significant loss of ductility. However, subsequent annealing at 350 °C to relieve the stresses provides an increase in ductility while maintaining high strength. A summary of the changes in mechanical properties is presented in **Table 2**.

As is seen from Table 1 and 2, the structural parameters of CP Ti Grade 4 differ significantly in various states and therefore may contribute differently to the strength properties of the material. The contributions of various microstructural parameters to the overall strength of the material are important to be calculated for establishing the basic mechanisms of hardening after the combined deformation-heat treatment of CP Ti Grade 4, as well as for understanding the nature of its superstrength state. Following works,^[16–19] the calculation may be realized by considering the additive contribution of such strengthening mechanisms as grain boundary (σ_{gb}), dislocation (σ_{dis}), solid solution (σ_{ss}), and dispersion (σ_{Or}) strengthening to the yield strength.

$$\sigma_y = \sigma_0 + \sigma_{gb} + \sigma_{dis} + \sigma_{ss} + \sigma_{Or} \quad (1)$$

where $\sigma_0 \approx 80$ MPa and is the frictional stress of the crystal lattice in Ti.^[20,21]

Following the known relations for these strengthening mechanisms such as grain boundary hardening (Hall–Petch strengthening), dislocation hardening, solid solution, and dispersion hardening (Orowan equation)] and considering the microstructural data in Table 2, the contributions of different strengthening mechanisms to UFG Ti strength were calculated. Their comparison with experimental data from mechanical tests is provided in **Table 3**.

Table 2. Mechanical properties of Ti Grade 4 in various structural states.

State ^{a)}	Microhardness, HV	$\sigma_{0.2}$ [MPa]	σ_u [MPa]	ϵ [%]
Hot rolled	237 ± 2	500	680	23.9 ± 1.4
HPT	353 ± 7	1020	1170	8.9 ± 1.2
HPT + 700	266 ± 5	600	720	30.8 ± 2.0
HPT + 700 + HPT	423 ± 8	1200	1340	0.9 ± 0.4
HPT + 700 + HPT + 350	433 ± 3	1340	1510	9.5 ± 2.0

^{a)} $\sigma_{0.2}$ – yield strength ; σ_u – ultimate tensile strength; ϵ – elongation to failure.

Table 3. Calculated contributions of various strengthening mechanisms to the strength of UFG Ti Grade 4 and experimental data on YS values for all analyzed states.

State	σ_y [MPa]	$\sigma_{y,calc}$ [MPa]	σ_0 [MPa]	σ_{gb} [MPa]	σ_{dis} [MPa]	σ_{ss} [MPa]	σ_{Or} [MPa]	σ_{SL} [MPa]
Hot rolled	500	480	80	140	150	110	0	0
HPT	1020	980		350	440		0	0
HPT + 700	600	600		200	140		70	0
HPT + 700 + HPT	1200	1170		400	380		0	200
HPT + 700 + HPT + 350	1340	830		340	150		150	0

Various strengthening mechanisms contribute to the strength of UFG Ti. However, their contributions in the state with the highest strength ($\sigma_y = 1340$ MPa) are noticeably less than this value, which means that the deformation of UFG Ti in such a state may also be affected by a different strengthening mechanism. Similar conclusions have been made for other UFG metallic materials, including Al alloys^[22,23] and a number of steels.^[24,25] Such a strengthening mechanism may be related to the state of grain boundaries in UFG materials, their non-equilibrium structure containing grain boundary dislocations and the grain boundary segregation of alloying elements.^[26,27]

Recent model calculations in work^[28] (**Figure 2**) that the formation of segregations of impurities or alloying elements at grain boundaries may significantly inhibit the dislocation nucleation at grain boundaries, thereby contributing to the additional hardening of UFG materials. Simultaneously, computer simulations^[29,30] and experimental studies^[13,22,23,25,31,32] provide convincing evidence of the formation of grain boundary segregations during the formation of UFG structures in metallic materials using SPD techniques. However, their nature and morphology are closely related to the processing regimes. This approximation allows for considering the difference between

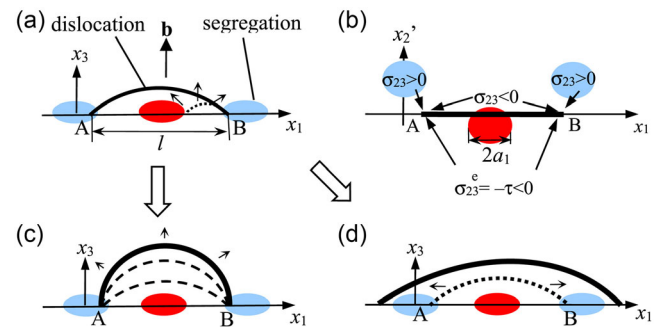


Figure 2. Expansion of a dislocation loop in the presence of segregations. The blue and red ovals denote the segregations that hinder and promote loop expansion, respectively. a, b) Dislocation loop ends, A and B, which nucleate and expand under the action of the applied load, are pinned by segregations. (a) Projection on dislocation glide plane illustrating segregation-induced pinning. (b) Projection on grain boundary plane illustrating the fact that a segregation can either promote or hinder dislocation loop expansion, depending on the sign of the x_2 -coordinate of its center. c) Dislocation loop expansion realized via its bow-out, thereby increasing the applied load if segregation-induced pinning is strong. d) If pinning is weak, loop expansion is realized via the unpinning and lateral motion of points A and B. Reproduced with permission.^[28] Copyright 2019, Elsevier.

the calculated and experimental data on YS values observed for the UFG Ti (Table 3).

This approach of obtaining high-strength titanium using combined SPD processing was used for producing long-sized rods intended for subsequent manufacture of medical implants. The original technique yields the rods up to 8 mm in diameter and 3 m in length from nanoTi using ECAP and/or ECAP-Conform followed by thermomechanical treatment (TMT), i.e., drawing and heat treatment.^[1,33] Such combined SPD treatment performed in this study results in the formation of a structure with a grain size of less than 150 nm in the UFG titanium rods (**Figure 3**). **Table 4** summarizes the mechanical properties of the initial and nanostructured Ti Grade 4 after ECAP-Conform and TMT. The high strength of nanoTi is also due to the formation of UFG structure and nanodispersed precipitates. The authors are currently analyzing the hardening mechanisms in nanoTi rods using quantitative methods.

2.2. Biomedical Studies

In biomedical applications, the osseointegration properties of Grade 4 titanium are as important as its strength. These properties depend on the surface characteristics of the material. Therefore, in this work we include a comparative analysis of the influence of surface etching on the osseointegration properties of Grade 4 titanium samples in the form of 10 mm long and 1 mm diameter needles. The samples were made from nanotitanium rods with UFG structure and were compared to the samples made of initial titanium with coarse-grained (CG) structure. The results reveal that, regardless of the initial material state (CG or UFG), mechanical polishing leads to a smooth, defect-free surface architecture. Etching forms a micro-roughened surface with pits and depressions. The surface morphology of the UFG sample is more homogeneous than that of the CG sample. A uniform distribution of “pits” with dimensions of $0.9 \pm 0.2 \mu\text{m}$ is revealed on the surface of the UFG sample. The surface of the CG sample has a disordered structure with pronounced drops in height, which are indicative of deep etching along the grain boundaries.

In addition to the boundaries, etching also exists intragranularly, which results in the formation of a pit structure. The etch pits on the surface of CG samples have an average size of $0.6 \pm 0.1 \mu\text{m}$ and are formed heterogeneously within individual grains with varying densities throughout the material.

As was noted in Section 5, the roughness parameters of the samples were studied in different states using a scanning probe

Table 4. Mechanical properties of conventionally processed and nanostructured Grade 4 Ti produced by ECAP-C and TMT. Data on Ti-6Al-4V ELI alloy are presented to compare.

Processing/ treatment terms	UTS [MPa]	YS [MPa]	Elongation [%]	Reduction of area [%]	Fatigue strength at 107 cycles
Conventional Ti (as received)	700	530	25	52	340
Nano-Grade 4	1230	1167	11	48	620
Annealed Ti-6Al-4V ELI	940	840	16	45	530

microscope NT-MDT Integra Prima and the modular program Gwyddion 2.11. The profilometry data was clarified through this study.

The etching treatment produced higher values for roughness parameters of both UFG and CG samples. To exclude the effect of severe etching of grain boundaries in the coarse-crystalline state, the roughness estimation of the CG-etched samples was performed inside the grains themselves without taking into account their boundaries. 3D image of the UFG sample is shown in **Figure 4**.

The main roughness parameters were determined for the materials in all states: R_a (the arithmetic mean of the departures of the profile) and R_q (mean value of measured departures from the mean line taken in the assessment length), as well as other amplitude parameters that characterize the surface based on vertical departures of roughness profile from the mean line: R_t (maximum profile height) and R_v (maximum valley depth on the roughness profile in the assessment length).^[34] For a clearer comparative evaluation of roughness, a histogram of R_a and R_q distribution was drawn according to the obtained results (**Figure 5**).

The highest values for roughness parameters were produced by the samples in the UFG etched state, the lowest values – by the samples in the UFG polished state (**Table 5**). The maximum average roughness R_a is $74 \pm 10 \text{ nm}$ in the etched UFG sample and the minimum is in the polished UFG sample - $17 \pm 3 \text{ nm}$. The etching of CG samples is not uniform and localized areas at different heights are observed.

Considering the morphology of tissue structures of the bone-implant interface (**Figure 6**), regardless of the surface topography, osseointegration occurred in all samples. At the first stage,

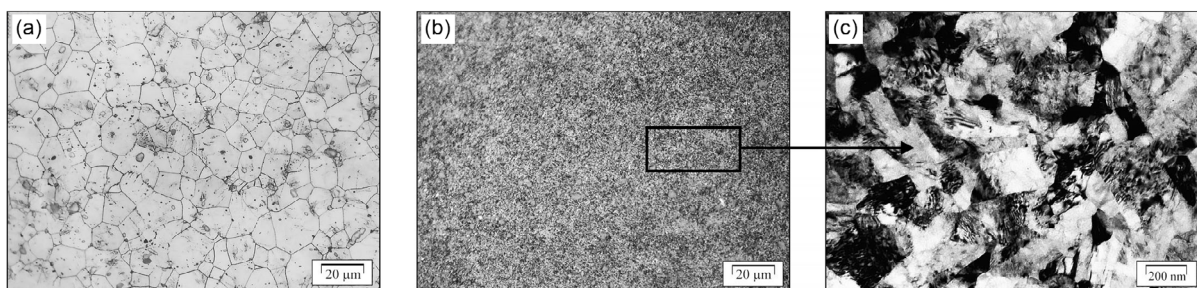


Figure 3. The microstructure of commercially pure titanium of Grade 4 a) in the initial hot-rolled state and b,c) after ECAP + TMT according to (a,b) optical microscopy and (c) TEM.

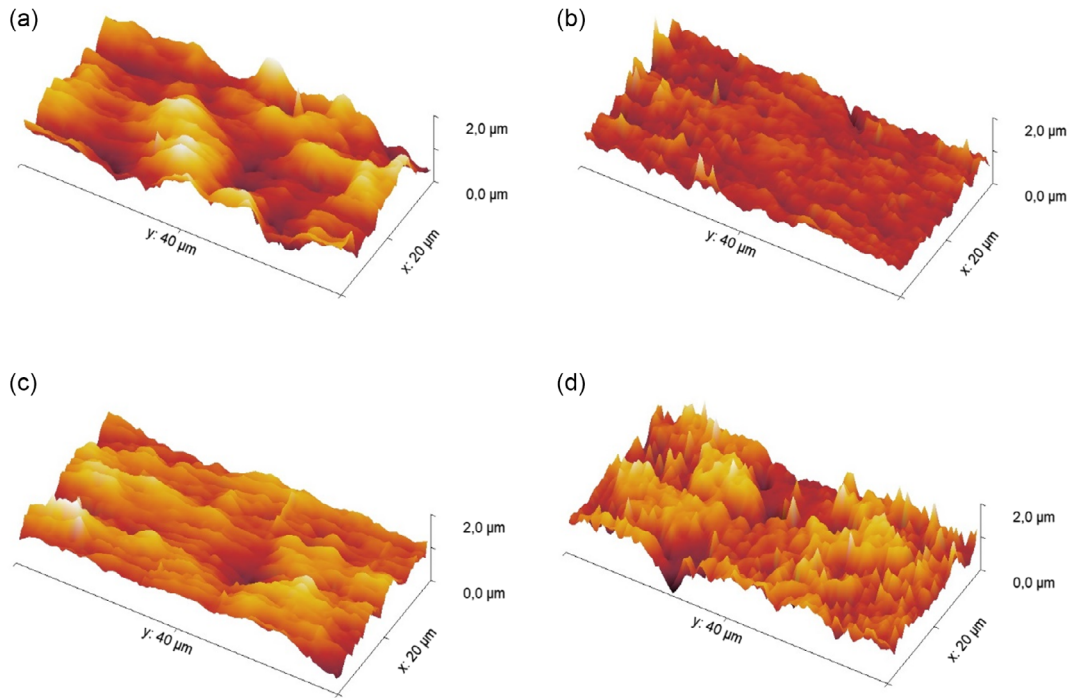


Figure 4. 3D images of data from a separately selected area: a) polished UFG sample; b) etched UFG sample; c) polished CG sample; d) etched CG sample.

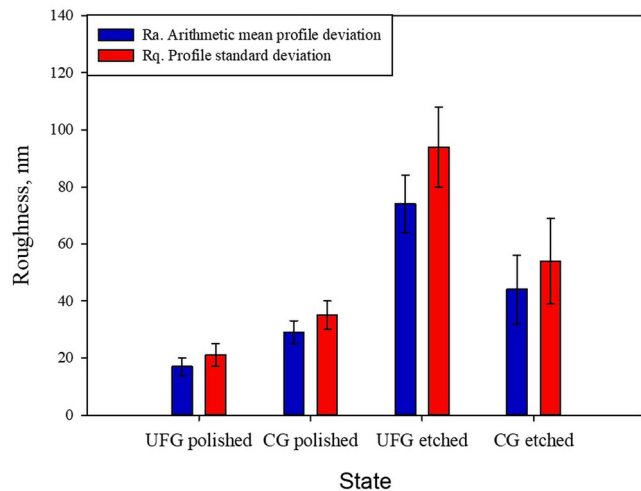


Figure 5. Histogram comparing roughness values for samples in different states.

Table 5. Roughness parameters values.

State	R_a [nm]	R_q [nm]	R_t [nm]	R_v [nm]
UFG polished	17 ± 3	21 ± 4	105 ± 10	58 ± 11
UFG etched	74 ± 10	94 ± 14	554 ± 140	286 ± 112
CG polished	29 ± 4	35 ± 5	184 ± 37	91 ± 25
CG etched	44 ± 12	54 ± 15	188 ± 58	104 ± 39

bone resorption was developing in the bone-implant contact area simultaneously with the newly-forming connective tissue, which then progressed into the mature, structurally organized coarse-fiber or fibrous connective tissue, subsequently transforming into cartilage and bone.

The SEM images show the most active formation of fibrous bone tissue on the samples with UFG surface (Figure 6a,b). At the same time, the most extensive bone formation was revealed on the UFG samples after chemical etching, where osteocytes and osteoblasts that form bone tissue are clearly observed (Figure 6b). Amount of bone tissue over $71.2\% \pm 12.4$ SD on the UFG etched samples was significantly larger compared to the UFG polished samples, for which similar index was less than $62.4\% \pm 8.3$ SD at a significance level of $p < 0.05$.

The study of osseointegration of CG samples with different surface treatments revealed that despite enhanced roughness parameters after etching (Figure 5), only cartilage tissue was formed in the bone-implant interface (Figure 6c,d). Observation of bone-implant interface of CG polished samples shows a layer of supra-cartilage and further, the formation of a zone of elastic cartilage tissue with groups of chondrocytes in the form of lined columns. The bone-implant interface analysis of the CG etched samples reveals many chondroblasts of the fibrous layer of cartilage tissue and young chondrocytes of newly formed cartilage tissue. The trabecular bone structure at the introduction of CG polished and CG etched implant samples is similar with mean values of 45.8 ± 6.5 SD and significance level of differences $p > 0.05$.

Figure 7 summarizes the rate ratios for tissues determined by morphological analysis of the bone-implant contact area for the

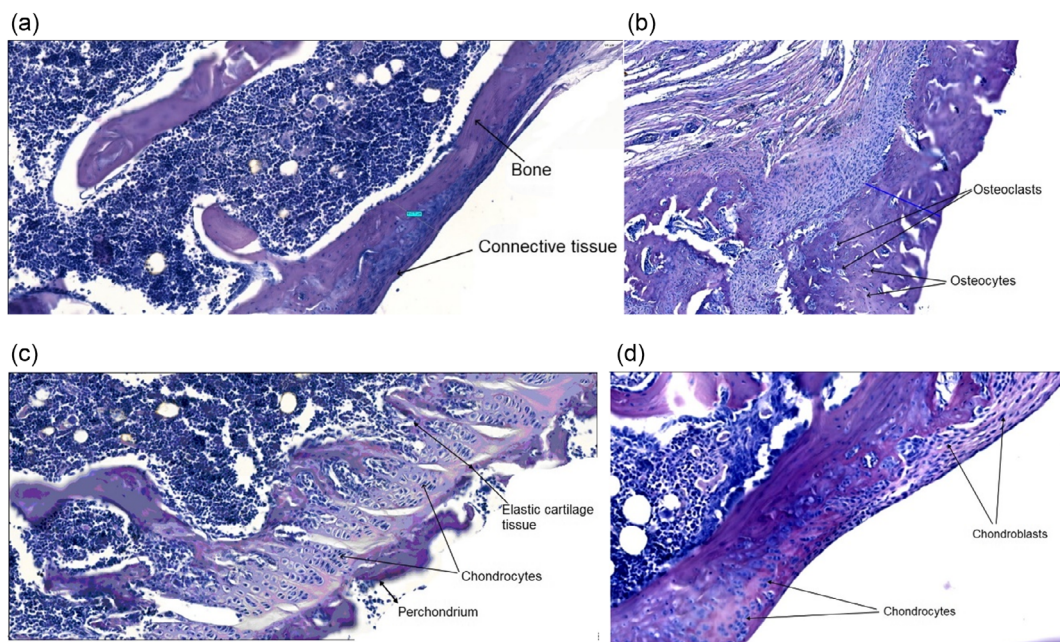


Figure 6. Bone–implant contact: a) UFG polished sample; b) UFG etched sample; c) CG polished sample; d) CG etched sample. Magnification x125.

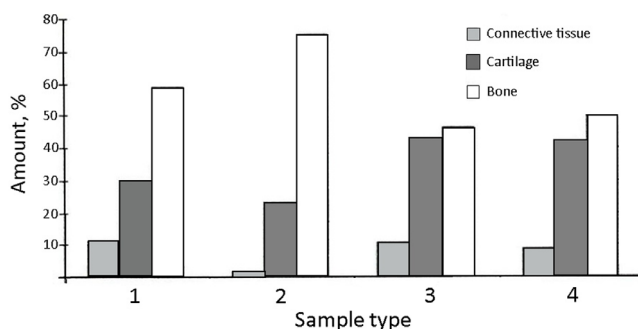


Figure 7. Comparison of tissue amount for inserted implants with different surface structures: 1 – UFG polished; 2 – UFG etched; 3 – CG polished; 4 – CG etched.

samples with different surfaces. The aforementioned results demonstrate that bone tissue regeneration on implants made of UFG Ti is significantly higher than on conventional CG Ti. Furthermore, the regeneration of nanoTi, following etching in the course of an 8 week experiment, reached a level of over 70%, indicating a state of reparative regeneration that is close to complete.

3. Discussion

Achievement of very high strength in CP Grade 4 titanium, the values of which are higher than the values of titanium alloys, by means of nanostructuring using the SPD techniques introduces new opportunities in the development and manufacture of medical implants with improved design. Currently, there are already first examples of nanoTi-based implants for dentistry

and maxillofacial procedures that are more miniature in size and have a number of advantages during and after surgery.^[1,3,35]

The studies herein on the physical nature of very high strength in nanoTi indicate that it is caused by the formation of ultrafine-grained structure during SPD processing, as well as the formation of nanoscale second-phase precipitates and grain boundary segregations of chemical elements present in titanium. The calculations conducted in the present study demonstrate that the latter factor also substantially contributes to achieving high strength in nanoTi with ultrafine grains. However, direct observations of the formation of segregations at grain boundaries are required, which may be implemented using 3D atomic tomography.^[20] Thus, the obtained results suggest that the strength properties of nanoTi are induced by several hardening mechanisms, which, however, are dependent on the modes of SPD processing. This approach is crucial for developing efficient technologies to obtain nanostructured titanium in various shapes (bars, bands, etc.) with exceptional mechanical properties required for a wide range of applications.

Another significant outcome of the present study is the enhanced osseointegration of nanoTi implants. As is known, implant topography has been shown to significantly influence cytological response of bone tissue cells.^[12,36,37] Nanotopography provides improved cell adhesion, chemical reactivity, and wettability during bone–implant contact.

The evidence from in vivo studies herein demonstrated that all implanted materials made of CP titanium were not toxic to living body tissues: no allergic reactions or side effects were observed. At the same time, etching of the samples resulted in improved osseointegration rates, and formation of UFG structure in titanium significantly increased positive effects on implant osseointegration. The amount of bone tissue in bone–implant interface

was much less on the CG samples than the amount on the UFG samples (Figure 7). This result correlates well with recent studies on medical plates for maxillofacial surgery obtained from nanoTi, where increased osseointegration of nanoTi implants was observed as well as low indicators of apoptosis of the osteoblasts and endothelial cells.^[35]

Such improved osseointegration of nanoTi samples is obviously related to several crucial factors. First, high density of grain boundaries in the UFG titanium may have a direct impact on cell attachment and proliferation.^[12] Further, the conducted studies have indeed shown the effects of UFG titanium etching on the formation of surface topography, which is the most optimal for in vitro biocompatibility due to increased cell adhesion and proliferation, which leads to improved biomedical properties in the interaction of the host tissue with the implant surface.^[37,38] Moreover, the formation of UFG structure in titanium with high density of grains boundaries is known to increase significantly the internal energy of the material and, as a result, may influence the morphology of the oxide film on the implant surface,^[13] which is also favorable for bone cells adhesion.^[1,2] This fact is also confirmed by the increase in the amount of bone tissue on the polished surface of UFG titanium compared to CG titanium (Figure 7).

At the same time, for the practical use of nano-implants, further in-vivo experiments with more profound analysis of the nature of increased osseointegration of nanoTi and the role of its surface modification are relevant.

4. Conclusion

The findings of this study suggest that severe plastic deformation techniques may profoundly enhance the mechanical strength of CP titanium. Although this material is highly desirable for medical applications, it is too soft for the manufacture of various products and such limitation may be overcome by nanostructuring using SPD techniques. Complex microstructural studies in this work reveal that such peculiar strengthening effect proceeds from a substantial grain refinement and the formation of an ultrafine-grained structure as well as from nanostructural features of grain boundaries, first of all - the segregations of different alloying elements at boundaries (Fe, O, N), induced by SPD processing. This approach is not only applicable to laboratory samples but also to obtaining semi-finished products in the form of nanoTi rods for manufacturing dental and maxillofacial implants. According to in-vivo studies on animals, nanoTi proved to be considerably more promising from an osseointegration point of view than its conventional counterpart, accelerating bone formation and healing around the implant sample. The findings that have been acquired so far indicate conclusively that nanoTi, especially with surface roughness, promote the best osseointegration by accelerating the bone formation in the bone-implant interface and has shown to be a very promising material for wide application in dentistry and maxillofacial surgery, where high-level requirements are critical to both mechanical and biofunctional properties of products. Moreover, the use of nanoTi in medicine offers new possibilities for miniaturizing implants and decreasing recovery period after surgery.

5. Experimental Section

Material Processing, Microstructural Analysis, and Mechanical Properties: In this work, the experiments were performed on commercially pure titanium Grade 4 produced by VSMPO-AVISMA Corporation (located in Verkhnyaya Salda, Russia) (chemical composition wt%: Fe - 0.37, N < 0.05, C - 0.005–0.008, H - 0.0001–0.0006; O - 0.32, rest - Ti). This material was processed by severe plastic deformation using the two most popular SPD techniques, particularly HPT, where substantial progress has been observed recently,^[11,39–43] and equal-channel angular pressing (ECAP), including its recent modification, ECAP-Conform.^[11,33] HPT-processed discs have an UFG structure with a diameter of 20 mm and a height of 1 mm with a grain size of about 100 nm. The details of processing are described in work.^[5] Using ECAP combined with the Conform process (ECAP-Conform) and subsequent drawing allowed for the formation of long-length UFG titanium rods with a diameter of 5 mm and a length of up to 3 m. Such rods make for semi-finished products that are suitable for precision numerically controlled machines to manufacture medical implants.^[1,33]

The microstructure of the samples was analyzed using a scanning electron microscope (SEM) JEOL JSM-6490LV (JEOL, Tokyo, Japan) at an accelerating voltage of 20 kV and a transmission electron microscope (TEM) JEOL JEM-2100 (JEOL, Tokyo, Japan) operating at an accelerating voltage of 200 kV.

X-ray phase analysis was performed using a Rigaku Ultima IV diffractometer (Rigaku Corporation, Tokyo, Japan) with CuK_α radiation in the range of 2θ scattering angles from 25° to 95° . The diffractograms were obtained using a parallel beam in the transmission, as described in detail in works.^[35,44]

Mechanical uniaxial static tensile tests were conducted at room temperature using an Instron 5982 testing machine (Instron, USA) with an initial strain rate of 10^{-4} s^{-1} . Similar to the technique used for microhardness measurement, specimens were cut from the middle radius zone of HPT-processed samples after different processing modes. Details of processing and samples' analysis are given in the work.^[5]

Surface Modification and Roughness Analysis: Special control implants for biomedical studies, 10 mm in length and 1 mm in diameter, were manufactured from the nanoTi rods. Surface properties of the implant samples were analyzed in different states: 1) nanostructured UFG titanium after polishing; 2) UFG titanium after chemical etching. For comparison, samples in the coarse-grained (CG) state were also studied: 3) CG state after polishing; and 4) CG state after chemical etching. For CG state, the initial hot-rolled material was heat-treated at 800°C with a holding time in the furnace of 15 min and cooling in air.

Samples were mechanically polished to "mirror-smooth" finish. Chemical etching was performed after polishing in $\text{NH}_4\text{OH}/\text{H}_2\text{O}_2$ solution.^[8] After etching, the samples were rinsed with distilled water and acetone and then air dried.

Surface structure was evaluated using a JEOL JSM-6490LV SEM. Surface roughness was assessed for all implants in this experiment. The roughness was quantified through the NT-MDT Integra Prima scanning probe microscope. The scanning type was probe scanning based on force interaction of a cantilever with a sharp probe on the end and the test surface. The resulting images were processed in the software Gwyddion 2.11 to determine the surface roughness parameters of the samples by 10 arbitrary lines for each state.^[45,46] In the experiment four main parameters of roughness were determined: R_a (arithmetic mean deviation of the profile), R_q (average value of the measured deviations from the mean line taken along the sampling length), R_t (maximum profile height), and R_v (maximum profile valley depth along the sampling length).^[34] Error analysis was performed using the standard evaluation method.^[47]

In Vivo Experiments: The implants' osseointegration was assessed on laboratory rats by introducing implant specimens 10 mm long and 1 mm in diameter. Experimental rats were acclimatized for at least 2 weeks before the experiment. All experiments on animals were conducted at the designated lab - the Laboratory of Cell Cultures, which has been successfully operating within Bashkir State Medical University (BSMU) on the related issues since 2014. The animal management, feeding, care, and

sacrifice were effected in strict compliance with the principles stated in the European Convention for the Protection of Vertebrate Animals Used for Experimental and Other Scientific Purposes (Strasbourg, France, 1986) and in accordance with the Rules of Good Laboratory Practice of the Russian Federation (Order of the Ministry of Health of the Russian Federation No. 199 n dated 01.04.2016) as well as with the guidelines for in vivo tests and the requirements of regulatory and technical documents governing research involving animals.^[6,9,35] All painful manipulations according to the local rules of laboratory practice had been made under ether anesthesia. All open surgical manipulations had been made with sterile surgical area, implants, and instrumentation.

Animals were anesthetized with intraperitoneal injection of a combination of ketamine (75 mg kg⁻¹) and silazine (10 mg kg⁻¹). Surgical area on the lower limb was isolated by shaving. Animals were laid supine on the stomach with external rotation and abduction of the lower limb. The patellar tendon was exposed under sterile conditions through skin incision followed by arthrotomy. The marrow canal was opened in the site of distal femoral metaepiphysis followed by the insertion of an implant. The tissue layers and skin were sutured. Bone-implant systems were retrieved after 8 weeks for morphological analysis.

For morphological analysis of tissue structures at the bone-implant interface, the samples were fixed with 4% paraformaldehyde buffer solution, decalcified with 10% acetic acid solution for 4 days, postfixed with 1% osmium tetroxide in 0.1 M cacodylate buffer for 1 h at 4 °C, dehydrated in graded alcohol, and embedded in epoxy resin followed by staining of sections with hematoxylin and eosin.^[9,36,48] Each tissue was stained blue-violet, differing from each other in the degree of brightness. The samples were examined using a SEM. The volume fraction of newly formed tissues (bone, cartilage, and connective tissues) was determined automatically using Adobe Photoshop software,^[37] with the contour-based identification of the areas occupied by tissues.

Experimental animals were sacrificed by overdosing on ether anesthesia.

Acknowledgements

The authors acknowledge the support in part from Russian Science Foundation (grant no. 22-19-00445) and in part by the Mega-grant State Program (agreement 075-15-2022-1114 dated by June 30, 2022).

Conflict of Interest

The authors declare no conflict of interest.

Data Availability Statement

The data that support the findings of this study are available from the corresponding author upon reasonable request.

Keywords

in vivo experiment, nanostructured titanium, osseointegration, strengthening mechanisms, surface modification, surface roughness

Received: February 15, 2024

Revised: July 8, 2024

Published online: July 23, 2024

[1] R. Z. Valiev, I. Sabirov, E. G. Zemtsova, E. V. Parfenov, L. Dluhoř, T. C. Lowe, in *Titanium in Medical and Dental Applications* (Eds: F. H. Froes, M. Qian), Woodhead Publishing, Duxford, UK **2018**, Ch. 4.3.

- [2] Y. Estrin, R. Lapovok, A. E. Medvedev, C. Kasper, E. Ivanova, T. C. Lowe, in *Titanium in Medical and Dental Applications* (Eds: F. H. Froes, M. Qian), Woodhead Publishing, Duxford, UK **2018**, Ch. 4.4.
- [3] R. Z. Valiev, E. V. Parfenov, L. V. Parfenova, *Mater. Trans.* **2019**, *60*, 1356.
- [4] R. Z. Valiev, E. A. Prokofiev, N. A. Kazarinov, G. I. Raab, T. B. Minasov, J. Strasky, *Materials* **2020**, *13*, 967.
- [5] E. I. Usmanov, L. R. Rezyapova, R. Z. Valiev, *Phys. Mesomech.* **2023**, *26*, 483.
- [6] F. L. Nie, Y. F. Zheng, S. C. Wei, D. S. Wang, Z. T. Yu, G. K. Salimgareeva, A. V. Polyakov, R. Z. Valiev, *J. Biomed. Mater. Res.* **2013**, *101A*, 1694.
- [7] A. S. de Souza, L. T. Colombo, H. Hadad, A. F. P. Santos, R. Capalbo da Silva, P. P. Poli, C. N. Elias, E. Vedovatto, F. A. Souza, P. S. P. de Carvalho, *J. Osseointegration* **2020**, *12*, 222.
- [8] D. V. Nazarov, V. M. Smirnov, E. G. Zemtsova, N. M. Yudintceva, M. A. Shevtsov, R. Z. Valiev, *ACS Biomater. Sci. Eng.* **2018**, *4*, 3268.
- [9] S. Svensson, F. Suska, L. Emanuelsson, A. Palmquist, B. Norlindh, M. Trobos, H. Bäckros, L. Persson, G. Rydja, M. Ohlander, B. Lyvén, J. Lausmaa, P. Thomsen, *Nanomedicine* **2013**, *9*, 1048.
- [10] A. B. Lemos, C. N. Elias, R. R. Bastos, E. F. Martinez, *Mater. Res.* **2021**, *24*, e20210147.
- [11] R. Z. Valiev, A. P. Zhilyaev, T. G. Langdon, *Bulk Nanostructured Materials: Fundamentals and Applications*, Wiley, Hoboken, NJ **2013**.
- [12] T. C. Lowe, R. A. Reiss, P. E. Illescas, C. F. Davis, M. C. Connick, J. A. Sena, *Mater. Res. Lett.* **2020**, *8*, 239.
- [13] M. M. Abramova, N. A. Enikeev, R. Z. Valiev, A. Etienne, B. Radiguet, Y. Ivanisenko, X. Sauvage, *Mater. Lett.* **2014**, *136*, 349.
- [14] I. Sabirov, M. Y. Murashkin, R. Z. Valiev, *Mater. Sci. Eng., A* **2013**, *560*, 1.
- [15] H. C. Wang, I. Shuro, M. Umemoto, *Mater. Sci. Eng., A* **2012**, *556*, 906.
- [16] M. Meyers, A. Mishra, D. Benson, *Prog. Mater. Sci.* **2006**, *51*, 427.
- [17] C. C. Koch, *Scr. Mater.* **2003**, *49*, 657.
- [18] I. Ovid'ko, R. Z. Valiev, Y. Zhu, *Prog. Mater. Sci.* **2018**, *94*, 462.
- [19] N. Balasubramanian, T. G. Langdon, *Metall. Mater. Trans. A* **2016**, *47*, 5827.
- [20] I. Semenova, G. Salimgareeva, G. Da Costa, W. Lefebvre, R. Valiev, *Adv. Eng. Mater.* **2010**, *12*, 803.
- [21] P. Luo, Q. Hu, X. Wu, *Metall. Mater. Trans. A* **2016**, *47*, 1922.
- [22] R. Valiev, N. Enikeev, M. Murashkin, V. Kazyskhanov, X. Sauvage, *Scr. Mater.* **2010**, *63*, 949.
- [23] P. V. Liddicoat, X. Z. Liao, Y. Zhao, Y. Zhu, M. Y. Murashkin, E. J. Lavernia, R. Z. Valiev, S. P. Ringer, *Nat. Commun.* **2010**, *63*, 1.
- [24] M. V. Karavaeva, S. K. Kiseleva, A. V. Ganeev, E. O. Protasova, M. M. Ganiev, L. A. Simonova, R. Z. Valiev, *J. Mater. Sci.* **2015**, *50*, 6730.
- [25] J. G. Kim, N. A. Enikeev, J. B. Seol, M. M. Abramova, M. V. Karavaeva, R. Z. Valiev, C. G. Park, H. S. Kim, *Sci. Rep.* **2018**, *8*, 11200.
- [26] R. Z. Valiev, B. Straumal, T. G. Langdon, *Annu. Rev. Mater. Res.* **2022**, *52*, 357.
- [27] R. Z. Valiev, *Mater. Trans.* **2014**, *55*, 13.
- [28] S. Bobylev, N. Enikeev, A. Sheinerman, R. Valiev, *Int. J. Plast.* **2019**, *123*, 133.
- [29] N. Q. Chinh, M. Y. Murashkin, E. V. Bobruk, J. L. Lábár, J. Gubicza, Z. Kovács, A. Q. Ahmed, V. Maier-Kiener, R. Z. Valiev, *Mater. Res. Lett.* **2021**, *9*, 475.
- [30] M. V. Petrik, A. R. Kuznetsov, N. A. Enikeev, Y. N. Gornostyrev, R. Z. Valiev, *Phys. Met. Metall.* **2018**, *119*, 607.
- [31] X. Sauvage, G. Wilde, S. Divinski, Z. Horita, R. Z. Valiev, *Mater. Sci. Eng., A* **2012**, *540*, 1.

- [32] X. Sauvage, A. Ganeev, Y. Ivanisenko, N. Enikeev, M. Murashkin, R. Z. Valiev, *Adv. Eng. Mater.* **2012**, *14*, 968.
- [33] D. V. Gunderov, A. V. Polyakov, I. P. Semenova, G. I. Raab, A. A. Churakova, E. I. Gimaltdinova, I. Sabirov, J. Segurado, V. D. Sitdikov, I. V. Alexandrov, N. A. Enikeev, R. Z. Valiev, *Mater. Sci. Eng., A* **2013**, *562*, 128.
- [34] A. I. Nicolas-Silvente, E. Velasco-Ortega, I. Ortiz-Garcia, L. Monsalve-Guil, J. Gil, A. Jimenez-Guerra, *Materials* **2020**, *13*, 314.
- [35] A. A. Matchin, E. V. Nosov, A. A. Stadnikov, G. V. Klevtsov, L. R. Rezyapova, N. A. Sayapina, E. V. Blinova, R. Z. Valiev, *ACS Biomater. Sci. Eng.* **2023**, *9*, 6138.
- [36] A. Wennerberg, T. Albrektsson, R. Jimbo, *Implant Surfaces and their Biological and Clinical Impact*, Springer, Heidelberg, Germany; New York, NY **2015**.
- [37] S. Bauer, P. Schmuki, K. von der Mark, J. Park, *Prog. Mater. Sci.* **2013**, *58*, 261.
- [38] V. V. D. Rani, K. Manzoor, D. Menon, N. Selvamurugan, S. V. Nair, *Nanotechnology* **2009**, *20*, 195101.
- [39] F. Wetscher, B. Tian, R. Stock, R. Pippan, *Mater. Sci. Forum* **2006**, *503–504*, 455.
- [40] A. Vorhauer, R. Pippan, *Scr. Mater.* **2004**, *51*, 921.
- [41] A. Bachmaier, A. Hohenwarter, R. Pippan, *Scr. Mater.* **2009**, *61*, 1016.
- [42] K. S. Kormout, R. Pippan, A. Bachmaier, *Adv. Eng. Mater.* **2017**, *19*, 1600675.
- [43] A. Bachmaier, R. Pippan, *Mater. Trans.* **2019**, *60*, 1256.
- [44] V. D. Sitdikov, R. K. Islamgaliev, M. A. Nikitina, G. F. Sitdikova, K. X. Wei, I. V. Alexandrov, W. Wei, *Philos. Mag.* **2019**, *99*, 73.
- [45] S. R. Yadhuraj, G. Satheesh Babu, M. Uttara Kumari, in *2016 3rd Int. Conf. on Advanced Computing and Communication Systems (ICACCS)*, Coimbatore, India, January **2016**, pp. 1–5.
- [46] P. Mehta, A. Sarma, A. D. Sivagami, N. HariPrakash, S. Gopi, B. Sarma, J. Ghosh, *Ind. J. Phys.* **2017**, *91*, 225.
- [47] J. R. Taylor, *An Introduction to Error Analysis: The Study of Uncertainties in Physical Measurements*, University Science Books, Sausalito, CA **1997**.
- [48] S. Facca, D. Lahiri, F. Fioretti, N. Messadeq, D. Mainard, N. Benkirane-jessel, A. Agarwal, *ACS Nano* **2011**, *5*, 4790.